High Internal Stresses in $Sr_{1-x}La_{1+x}Al_{1-x}Mg_xO_4$ Solid Solution ($0 \leq x \leq 0.7$) Characterized by Infrared and Raman Spectroscopies Coupled with Crystal Structure Refinement

A. Magrez,*,† M. Cochet,‡ O. Joubert,† G. Louarn,‡ M. Ganne,† and O. Chauvet‡

Laboratoire de Chimie des Solides and Laboratoire de Physique Cristalline, Institut des Matériaux Jean Rouxel, Université de Nantes, UMR 6502, 2 rue de la Houssinière, BP 32229, 44322 Nantes Cedex 3, France

Received October 25, 2000. Revised Manuscript Received May 7, 2001

The $Sr_{1-x}La_{1+x}Al_{1-x}Mg_xO_4$ ($0 \leq x \leq 0.7$) solid solution with the K_2NiF_4 structure has been prepared by a new "Chimie Douce" route for the first time. The crystal structures have been refined, from X-ray diffraction patterns, in a tetragonal lattice with the *I*4/*mmm* space group. The evolution of Raman and infrared spectra as a function of the composition and the excitation wavelength are observed. These results are discussed on the basis of the interatomic distances. An assignment of the Raman and IR spectra is given for all the compositions.

Introduction

Ruddlesden−Popper (R−P) phases of nominal composition $M_2[A_{n-1}B_nO_{3n+1}]$ have been attracting much attention for a few decades now.[1,2] These phases consist of M cations interleaving layers with composition $[A_{n-1}B_nO_{3n-1}]$.[3−5] Depending on their composition, they present a lot of interesting physical and chemical properties: protonic conduction,[6,7] oxygen diffusion,[8−11] electronic transport,[12−15] complex magnetic order,[16−19] catalytic activities,[20−23] etc. In this family, $SrLaAlO_4$ has a two-dimensional perovskite K_2NiF_4 structure. It can be described in a tetragonal lattice with a *I*4/*mmm* space group. The structure consists of a sequence of one perovskite layer (AlO_2) alternating with two rock salt (Sr,LaO) layers. Sr/La cations are 9-fold coordinated while Al^{3+} has an octahedral coordination.

In this paper, we explore the $Sr_{1-x}La_{1+x}Al_{1-x}Mg_xO_4$ solid solution ($0 < x < 1$) which is derived from $SrLaAlO_4$. The stabilization of the structure of the solid solution requires a bond length matching across the intergrowth interface. It is usually discussed in terms of the Goldschmidt tolerance factor *t* defined as

$$t = d_{Sr/La-O}/\sqrt{2}d_{Al/Mg-O}$$

$d_{Sr/La-O}$ and $d_{Al/Mg-O}$ represent the mean equilibrium bond lengths between metal atoms and oxygen given by the sum of the room-temperature ionic radii. As shown in Figure 1, the *t* value derived for the $Sr_{1-x}La_{1+x}Al_{1-x}Mg_xO_4$ solid solution is close to unity and is expected to be stable in a large composition range.

We aim at investigating this composition range. $Sr_{1-x}La_{1+x}Al_{1-x}Mg_xO_4$ ($0 \leq x \leq 1$) are synthesized by a "chimie douce" route. X-ray diffraction showed that the solid solution is stable in the $0 \leq x \leq 0.7$ range. A significant evolution of the interatomic distances is deduced from the structure refinements. It is related to the regular evolution of *t* with *x*. We suggest that it is associated with the building of internal stresses which

* To whom correspondence should be addressed. Phone: (33)2/40/37/39/36. Fax: (33)2/40/37/39/95. E-mail: Magrez@cnrs-imn.fr.
† Laboratoire de Chimie des Solides.
‡ Laboratoire de Physique Cristalline.

(1) Turrillas, X.; Sellars, A. P.; Steele, B. C. H. *Solid State Ionics* **1988**, *28−30*, 465.
(2) Gopalakrishnan, J.; Bhat, V. *Inorg. Chem.* **1987**, *26*, 4299.
(3) Ruddlesden, S. N.; Popper, P. *Acta Crystallogr.* **1957**, *10*, 538.
(4) Ruddlesden, S. N.; Popper, P. *Acta Crystallogr.* **1958**, *11*, 54.
(5) Ganguly, P.; Rao, C. N. R. *J. Solid State Chem.* **1984**, *53*, 193.
(6) Shimura, T.; Suzuki, K.; Iwahara, H. *Solid State Ionics* **1997**, *104*, 79.
(7) Steele, B. C. H. *Mater. Sci. Eng.* **1992**, *B13*, 79.
(8) Jorgensen, J. D.; Dabrowski, B.; Pei, S. *Phys. Rev.* **1989**, *B40*, 2187.
(9) Hiroi, Z.; Takano, M.; Bando, Y. *Supercond. Sci. Technol.* **1991**, *4*, 139.
(10) Subramanian, M. A.; Crawford, M. K.; Harlow, R. L.; Ami, T.; Fernandez-Baca, J. A.; Wang, Z. R.; Johnston, D. C. *Physica C (Amsterdam)* **1994**, *235−240*, 743.
(11) Shimura, T.; Suzuki, K.; Iwahara, H. *Solid State Ionics* **1999**, *125*, 313.
(12) Bednorz, J. G.; Müller, K. A. *Z. Phys.* **1986**, *B64*, 189.
(13) Toda, K.; Teranishi, T.; Sato, M. *J. Eur. Ceram. Soc.* **1999**, *19*, 1525.
(14) Omata, T.; Hoshino, S.; Ikawa, H.; Sasamoto, T. *J. Ceram. Soc. Jpn.* **1995**, *103*, 1297.
(15) Omata, T.; Ueda, K.; Hosono, H.; Katada, M.; Ueda, N.; Kawazoe, H. *Phys. Rev.* **1994**, *B49*, 10194.
(16) Martínez, J. L.; Prieto, C.; De Andrés, A.; Rodríguez-Carvajal, J.; Vallet-Regí, M.; González-Calbet, J. M. *J. Magn. Magn. Mater.* **1995**, *140−144*, 179.
(17) Chauvet, O.; Goglio, G.; Molinié, P.; Corraze, B.; Brohan, L. *Phys. Rev. Lett.* **1996**, *81*, 1102.
(18) Romero de Paz, J.; Martínez, J. L.; Sáez Puche, R. *J. Alloys Compd.* **2000**, *303−304*, 293.
(19) Mizuno, N.; Yamato, M.; Tanaka, M.; Misono, M. *Chem. Mater.* **1989**, *1*, 232.
(20) Halasz, I.; Brenner, A.; Shelf, M.; Simon, Ng K. Y. *Catal. Lett.* **1991**, *11*, 327.
(21) Yasuda, H.; Nitadon, T.; Mizuno, N.; Misono, M. *Bull. Chem. Soc. Jpn.* **1993**, *66*, 3492.
(22) Teraoka, Y.; Nakano, K.; Shangguan, W.; Kagawa, S. *Catal. Today* **1996**, *27*, 107.
(23) Wu, Y.; Zhao, Z.; Liu, Y.; Yang, X. *J. Mol. Catal. A* **2000**, *155*, 89.

10.1021/cm001209e CCC: $20.00
Published on Web 10/16/2001

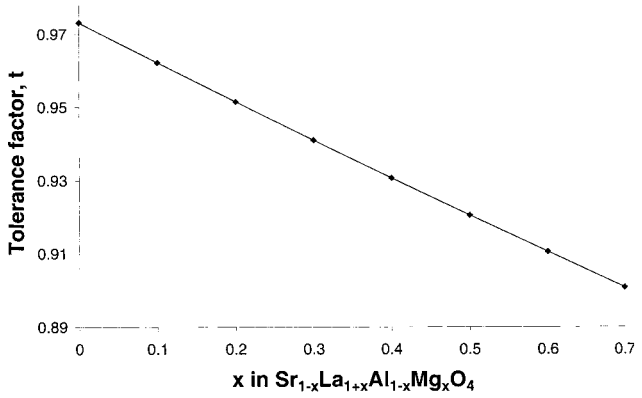

Figure 1. Variation of the tolerance factor with x in $Sr_{1-x}La_{1+x}Al_{1-x}Mg_xO_4$. The values are based on 9-fold coordinated ionic radii for La^{3+} and Sr^{2+} and 6-fold coordinated ionic radii for Al^{3+} and Mg^{2+}.

are evidenced by Raman scattering and infrared absorption. Optical phonon modes are assigned from the spectroscopic studies.

Experimental Section

Synthesis. To circumvent several drawbacks of the ceramic synthesis method,[24,25] we used a novel "Chimie Douce" synthesis route. It is well established that decomposition of precursors with small particle size and high surface area often favors the preparation of homogeneous phases which are inaccessible by conventional solid-state reactions.

Aqueous solution of $Sr(NO_3)_2$ (Fluka, 99%), $La(NO_3)_3{\cdot}6H_2O$ (Fluka, 99%), $Al(NO_3)_3{\cdot}6H_2O$ (Fluka, 99%), and $Mg(NO_3)_3{\cdot}9H_2O$ (Fluka, 99%) were mixed in the required stoichiometric ratios. To complex the cations, 11-aminoundecanoic acid (Fluka, 98%) was added. The resulting solution was gelled at 373 K using acrylamide (Fluka, 99.5%) to form an organic polymer network.[26] This gel was dried in a simple microwave furnace for 20 min. Heating the resulting solid to around 473 K leads to spontaneous combustion, yielding an oxidic product in fine particulate form. The free organic white powder, so obtained, was pressed into cylindrical pellets and heat treated in air at 1673 K for 12 h.

X-ray and Spectroscopic Characterization. The X-ray powder diffraction (XRPD) patterns of the compounds were recorded at room temperature in Debye−Scherrer geometry using an INEL position-sensitive detector with monochromatized Cu $K\alpha_1$ radiation. A very homogeneous thin layer of powder was put on the external side of a thin Lindeman capillary whose surface was made sticky by means of modeling clay to prevent high absorption coefficient of the samples. Structure refinements were carried out by the Rieltveld method using the program FULLPROF.[27]

Raman spectra were recorded on a multichannel Jobin-Yvon T64000 spectrometer. Different excitation lines used for this study were 363, 457.9, 514.5, and 676.4 nm. Normal scattering geometry (for the 363-nm excitation) and backscattering configuration (for other wavelengths) were used. Raman spectra with 1064-nm Nd:YAG laser excitation were also obtained with a FT Raman Bruker RFS 100 spectrometer in the backscattering geometry. All experiments were performed at room temperature on powdered samples.

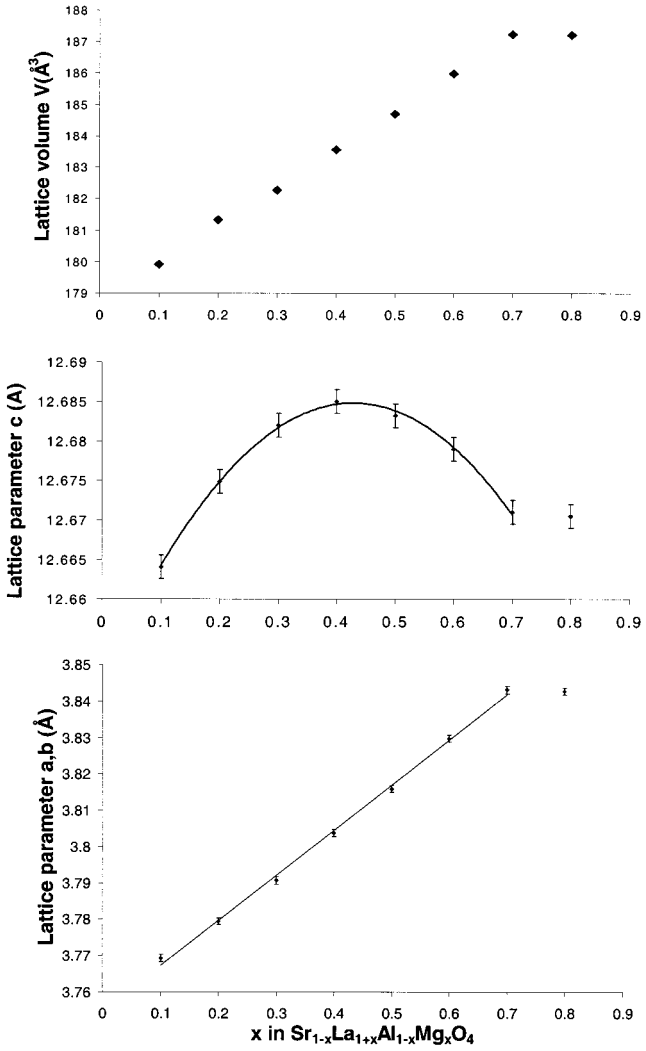

Figure 2. Cell parameters and volume versus x in $Sr_{1-x}La_{1+x}Al_{1-x}Mg_xO_4$. The upper limit of the solid solution is $x \approx 0.7$.

A Nicolet 20 SXC Fourier transform infrared spectrophotometer was used for infrared absorption in the 400−4000-cm^{-1} wavenumber range. The room-temperature IR spectra were measured using KBr pressed pellets. They were corrected for the substrate absorption.

Results and Discussion.

Solid Solution Range. $Sr_{1-x}La_{1+x}Al_{1-x}Mg_xO_4$ crystallizes in a tetragonal cell with the *I*4/*mmm* space group. The room-temperature evolution of a (= b) and c lattice parameters along with the lattice volume V are given for each composition in Figure 2.

The cell parameter a increases almost linearly with x up to $x = 0.7$, from 3.77 to 3.84 Å, which is more than 0.07 Å, whereas the cell parameter c varies only by 0.02 Å in the above-mentioned compositional range. When $x = 0.8$, two impurity phases, namely, La_2O_3 and MgO, were detected.

The $Sr_{1-x}La_{1+x}Al_{1-x}Mg_xO_4$ solid solution has thus a stable composition range, $0 \le x \le 0.7$ ($SrLaAlO_4$[28]). Probably, this is the first time that this solid solution is obtained over such a wide compositional range. This

(24) Rao, C. N. R.; Raveau, B. In *Transition Metal Oxides*; VCH Publishers, Inc.: New York, 1995.
(25) In *Soft Chemistry Route to New Materials-Chimie Douce*, proceedings of the international symposium held in Nantes, France, Sept 6−10, 1993; Rouxel, J., Tournoux, M., Brec, R., Eds.; Materials Science Forum; 1994; *Trans Tech Publications*: pp 152−153.
(26) Douy, A.; Odier, P. *Mater. Res. Bull.* **1989**, *24*, 1119.
(27) Roisnel, T.; Rodriguez-Carjaval, J. *FULLPROF*, LLB−Saclay LCSIM-Rennes, May 2000, *Physica B* **1993**, *192*, 55.
(28) Shannon, R. D.; Oswald, R. A.; Parise, J. B.; Chai, B. H. T.; Byszewski, P.; Pajaczkowska, A.; Sobolewski, R. *J. Solid State Chem.* **1992**, *98*, 90.

Table 1. Parameters and *R* Factors from the Rietveld Refinement

		$x = 0$[28]	$x = 0.1$	$x = 0.2$	$x = 0.3$	$x = 0.4$	$x = 0.5$	$x = 0.6$	$x = 0.7$
cell parameters (Å)	a	3.7564(1)	3.76932(9)	3.78254(7)	3.79121(8)	3.80413(9)	3.81611(2)	3.83002(8)	3.84414(9)
	c	12.6357(4)	12.6641(5)	12.6749(5)	12.6821(4)	12.6852(4)	12.6832(5)	12.6793(5)	12.6710(6)
Sr/La (0, 0, z)	z	0.35885(2)	0.35939(7)	0.36009(9)	0.36054(8)	0.36079(7)	0.36092(8)	0.36159(8)	0.36179(9)
	B_{iso} (Å^2)	0.4(1)	0.73(2)	1.14(3)	1.33(3)	1.20(8)	1.40(9)	1.39(2)	1.21(3)
Al/Mg (0, 0, 0)	B_{iso} (Å^2)	0.5(1)	1.09(9)	1.3(1)	1.4(1)	1.19(8)	1.45(9)	1.6(1)	1.2(1)
O(1) ($^1/_2$, 0, 0)	B_{iso} (Å^2)	0.5(1)	0.8(1)	0.9(2)	2.2(2)	1.0(1)	1.2(1)	1.5(1)	0.8(2)
	z	0.1625(4)	0.1653(4)	0.1656(6)	0.1685(5)	0.1690(5)	0.1713(5)	0.1712(5)	0.1738(6)
O(2) (0, 0, z)	B_{iso} (Å^2)	0.9(1)	1.1(1)	1.4(2)	1.7(1)	1.7(1)	1.6(1)	1.7(1)	2.1(2)
	R_{bragg}		4.03%	4.39%	3.26%	3.73%	2.69%	2.92%	4.87%
	R_{wp}		8.57%	10.3%	8.98%	8.19%	7.53%	7.34%	9.89%
	R_{exp}		2.95%	5.90%	3.65%	3.13%	3.56%	2.61%	4.39%

Table 2. Selected Interatomic Distances (Å) (Standard Deviations Are Given in Parentheses)

	$x = 0$	$x = 0.1$	$x = 0.2$	$x = 0.3$	$x = 0.4$	$x = 0.5$	$x = 0.6$	$x = 0.7$
Al/Mg O(1)	1.878(1)	1.884(1)	1.891(1)	1.895(1)	1.902(1)	1.908(1)	1.915(1)	1.922(1)
Al/Mg O(2)	2.053(5)	2.093(1)	2.098(1)	2.137(1)	2.144(1)	2.173(1)	2.17(1)	2.203(1)
Sr/La O(1)	2.59(1)	2.593(1)	2.593(1)	2.592(1)	2.595(1)	2.599(1)	2.597(1)	2.60(1)
Sr/La O(2)$_m$	2.670(1)	2.683(1)	2.694(1)	2.706(1)	2.716(1)	2.729(1)	2.74(1)	2.755(1)
Sr/La O(2)	2.481(5)	2.459(1)	2.466(1)	2.435(1)	2.433(1)	2.405(1)	2.414(1)	2.382(1)

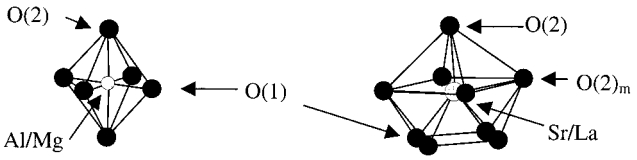

Figure 3. Al/MgO_6 and Sr/LaO_9 polyhedrons, which describe the K_2NiF_4-type structure.

upper limit of composition ($x = 0.7$) sets a limit to the tolerance factor t close to 0.9 (see Figure 1), which is higher than the value suggested in the literature.[29]

The evolution of the lattice parameter a with x is likely due to the increase of the ionic radii of the Mg^{2+}/Al^{3+} cation from 0.535 to 0.665 Å, which is indeed related to the decrease of the t factor. Since the c parameter is not significantly affected (see Figure 2), the lattice volume expansion is quite similar to the a parameter increase. The small evolution of the c parameter with a maximum around $x = 0.5$ can be explained by the mismatch, which results in accommodating the perovskite layer between rock salt layers.

Crystal Structure of $Sr_{1-x}La_{1+x}Al_{1-x}Mg_xO_4$. The structure of the $Sr_{1-x}La_{1+x}Al_{1-x}Mg_xO_4$ solid solution ($0.1 \leq x \leq 0.7$) was refined, using as a starting point the $SrLaAlO_4$ ($x = 0$) atomic positions in the $I4/mmm$ space group (D_{4h}^{17}).[28] Sr^{2+} and La^{3+} ions, along with Al^{3+} and Mg^{2+}, were statistically distributed over the 4e (C_{4v} symmetry) and 2a (D_{4h} symmetry) Wyckoff positions. The results of the refinement are given in Table 1.

The structure is built from Al/MgO_6 octahedra and Sr/LaO_9 dodecahedra sketched in Figure 3. The perovskite planes are obtained from the connection of the octahedra via the equatorial O(1) oxygen (in D_{2h} symmetry). The two apical O(2) oxygens (in C_{4v} symmetry) connect the perovskite layers with the rock salt ones along the c axis. The Sr/LaO_9 dodecahedron involves four equatorial oxygen O(2)$_m$, at approximately the same z position ($z = 0.34$), one apical O(2) close to $z = 0.16$ and four O(1) at $z = 0$.

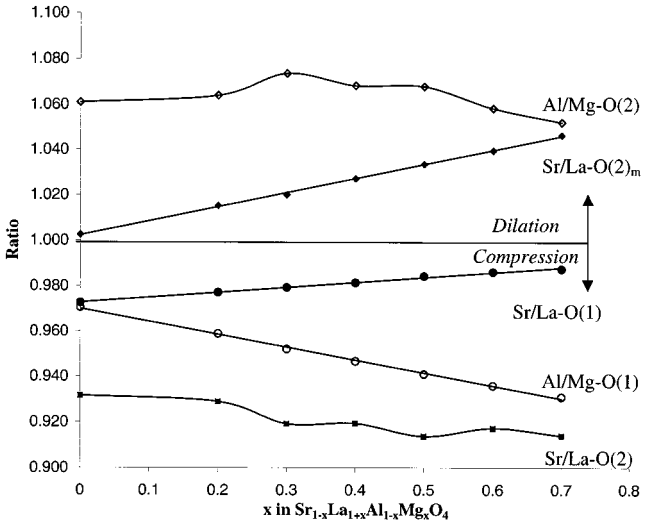

Figure 4. Compression and/or dilation effects of the five different bonds versus x in $Sr_{1-x}La_{1+x}Al_{1-x}Mg_xO_4$.

From the structure refinement, we can extract the cation−oxygen interatomic distances. Table 2 shows various interatomic distances and from these results the following inferences can be drawn:

(i) The perovskite layer is elongated along the c axis ($d_{Al/Mg-O(2)} \gg d_{Al/Mg-O(1)}$).

(ii) Increasing the La/Mg content (x parameter) leads to an elongation of the equatorial distance Al/Mg−O(1).

(iii) On the other hand, the Sr/La−O(2)$_m$ distance is longer than the Sr/La−O(2) distance, which suggests a compression of the dodecahedra along the c direction. This effect is enhanced as x increases.

A compression and/or dilation ratio of the five different "cation−oxygen" bonds can be deduced from the ratio of the actual distance (determined from Table 2) to the ideal distance defined as the sum of the room-temperature ionic radii (Sr^{2+}, $r = 1.31$ Å; La^{3+}, $r = 1.216$ Å; Al^{3+}, $r = 0.535$ Å; Mg^{2+}, $r = 0.720$ Å; O^{2-}, $r = 1.40$ Å[30]). As inferred from Figure 4, the Al/MgO_6 octahedra are stretched along the c axis while the Sr/LaO_9 dodeca-

(29) Goldschmidt, V. M.; Det Norske Videnskaps-Akodemi, I. Materm. Naturvid. Klasse; 1926; no. 2.

(30) Shannon, R. D. *Acta Crystallogr.* **1976**, *A32*, 751.

hedra are compressed. Indeed, it is tempting to investigate such a strained structure by vibrational spectroscopy, which is sensitive to the local bonding.

Normal-Modes Analysis. We need to identify the phonon modes of $Sr_{1-x}La_{1+x}Al_{1-x}Mg_xO_4$, which obey the vibrational selection rules prior to the experimental analysis. This is performed using group theory within the nuclear site group analysis scheme.[31] This site group analysis in the solid solution crystal structure (D_{4h}^{17}) gives the following vibrational representation:

$$\text{Sr/La} \rightarrow C_{4v} \rightarrow A_{1g} + E_g + A_{2u} + E_u$$

$$\text{Al/Mg} \rightarrow D_{4h} \rightarrow A_{2u} + E_u$$

$$\text{O(1)} \rightarrow D_{2h} \rightarrow A_{2u} + B_{2u} + 2E_u$$

$$\text{O(2)} \rightarrow C_{4v} \rightarrow A_{1g} + E_g + A_{2u} + E_u$$

$$\Gamma = 2A_{1g} + 2E_g + 4A_{2u} + 5E_u + B_{2u}$$

Four Raman active optical modes of symmetry A_{1g} and E_g result from oscillations of O(2) and Sr/La atoms. The $3A_{2u} + 4E_u$ modes are IR active. One A_{2u} and one E_u are acoustic modes. The B_{2u} mode is silent.

Raman Scattering. Several Raman studies of $SrLaAlO_4$ have been reported.[32−34] Most of them have been performed on a single crystal, which allow the use of polarization to discriminate between the different modes. However, a complete assignment of the optical phonons in Raman spectroscopy is not yet fully established.

We present in Figure 5. the Raman spectra obtained at $\lambda_{exc} = 514.5$ nm for powder samples with composition ranging from $x = 0$ (a) to $x = 0.7$ (h). In Figure 6, the frequencies are plotted as functions of composition. The spectrum of $SrLaAlO_4$ ($x = 0$, spectrum (a)) is dominated by two main bands observed at 221 and 290 cm^{-1} and three additional weak bands around 128, 440, and 584 cm^{-1}. All these bands can be observed in spectra (a)−(h), but they show a significant evolution both in frequencies and relative intensities. Hadjiev et al.[34] observed also five bands with different polarizations on $SrLaAlO_4$ single crystals using 514-nm excitation. The three central bands at 222, 301, and 442−446 cm^{-1} are observed at the same position as ours; however, they found a low-frequency band at 155 cm^{-1} and a high-frequency one at 512 cm^{-1}. The origin of this discrepancy is unclear. They suggested that the 301- and 512-cm^{-1} bands involve oscillations of O(2) atoms while the 155- and 222-cm^{-1} ones are derived from the Sr/La oscillations. The band around 444 cm^{-1} is attributed to a second-order scattering from an overtone of the phonon at 222 cm^{-1}.

We observe a wide band, which downshifts from 128 to 95 cm^{-1} (≈26%) for $x = 0$ to $x = 0.7$, respectively. This band is related, in E_g symmetry, to the vibration of the Sr/La−$O(2)_m$ bond in the *ab* plane of the lattice.

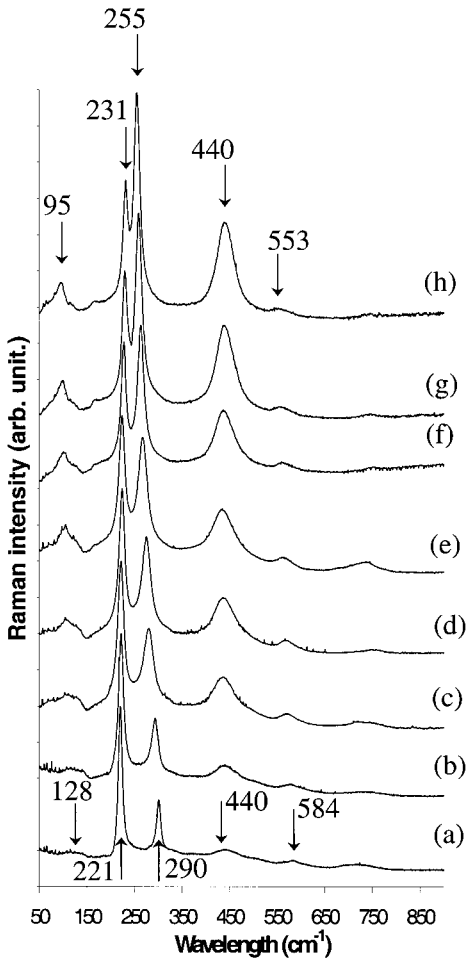

Figure 5. Raman spectra from $x = 0$ (a) to $x = 0.7$ (h) recorded at 514.5 nm.

Indeed, the substitution of Sr^{2+} by La^{3+} leads to an increase of the molar weight. However, a rough calculation shows that it contributes only for ≈1%. The frequency shift can be related to the Sr/La−$O(2)_m$ bond dilation shown in Figure 4. The increase of the bond dilation is associated to a weakening of the bond, which results in a diminution of the frequency. Within the harmonic approximation we expect a diminution (≈10%) of the frequency related to the weakening of the bond. It is of the correct order of magnitude and supports our assignment.

The very strong band observed at 221 cm^{-1} is for $x = 0$ and for $x = 0.7$ at 231 cm^{-1}. This band is assigned to the vibration of the Sr/La−O(2) bond along the *c* axis in the A_{1g} configuration. As noted previously, the mass effect is not very effective (≈1%). This moderate increase of the frequency during the increase of *x* can be explained by the increase of the compression of Sr/La−O(2). This increase (≈2%) is due to a strengthening of the bond which upshifts the resonance frequency by ≈4% in the harmonic approximation, that is, within the order of magnitude of our observations.

So we can conclude that these two bands are due to the two internal vibrations of the "Sr/LaO_9" dodecahedron and their evolution with the parameter *x* is related to the stress effects as discussed above.

In contrast, the two bands at 290 and 440 cm^{-1} can be assigned to the bridge M−O−M oxygen bonds between two building blocks of the structure. Here also,

(31) Rousseau, D. L.; Bauman, R. P.; Porto, S. P. S. *J. Raman Spectrosc.* **1981**, *10*, 253.
(32) Ryba-Romanovski, W.; Golab, S.; Hanuza, J.; Maczka, M.; Pietraszko, A.; Berkowski, M.; Pajaczkowska, A. *J. Phys. Chem. Solids* **1991**, *52*, 1043.
(33) Drozdowski, M.; Kozielski, M.; Pajaczkowska, A. *Acta Phys. Pol. A* **1997**, *92*, 177.
(34) Hadjiev, V. G.; Carbona, M.; Ivanov, I.; Popov, V.; Gyulmezov, M.; Illiev, M. N.; Berkowski, M. *J. Alloys Compd.* **1997**, *251*, 7.

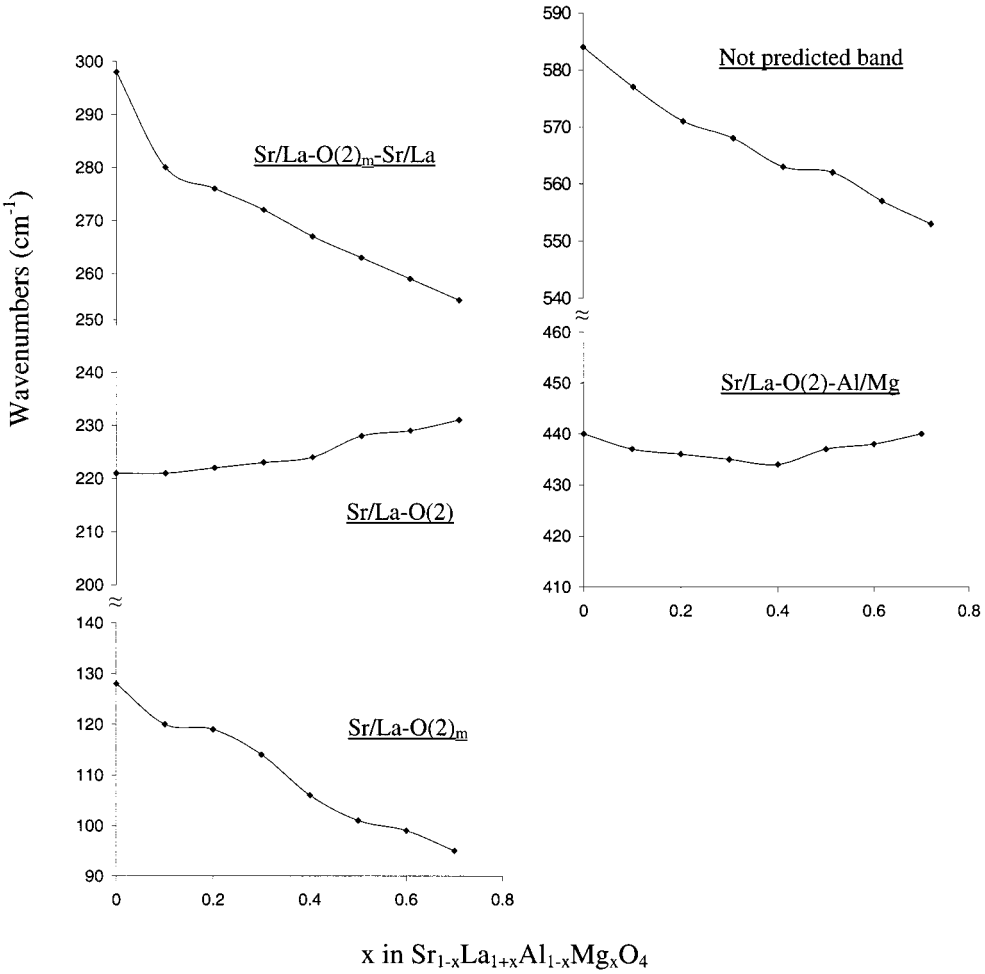

Figure 6. Raman frequencies of the five bands, observed at 514.5 nm, plotted versus x in $Sr_{1-x}La_{1+x}Al_{1-x}Mg_xO_4$.

the same kind of consequence as previously observed is expected.

The band at 290 cm^{-1} in the spectrum of $x = 0$ shifts down to 255 cm^{-1} for the sample with $x = 0.7$. This band corresponds to the vibration of the bridge Sr/La−$O(2)_m$−Sr/La oxygen bond in E_g symmetry. The downshift of the frequency is caused by the dilation of the bond of Sr/La−$O(2)_m$ and the increase of the a parameter with the substitutional ratio.

The next band is located around 440 cm^{-1} for all spectra. This band is related to the vibration of the bridge Sr/La−O(2)−Al/Mg oxygen bond along the c axis in A_{1g} symmetry. Two effects counterbalance: the decrease of the dilation of the bond of Al/Mg−O(2) and the increase of the compression of the Sr/La−O(2) bond.

We can outline a band observed at 584 cm^{-1} for the $x = 0$ sample and at 564 cm^{-1} in the $x = 0.7$ spectrum. This band is not predicted by the normal-mode analysis and can be attributed to a local distortion of the Al/MgO_6 octahedron. A Raman study of the $x = 0.5$ compound was carried out for different excitation lines from 363 nm (UV) to 1064 nm (FT Raman). Resonance effects are observed for this sample, especially at 363 nm. The enhancement in the bands at 273, 444, and 572 cm^{-1} also indicate resonance effects. This resonance effect confirms the assignment of the Raman study at 514.5 nm.

Thus, we assign the five Raman bands based on structural modifications and resonance effects.

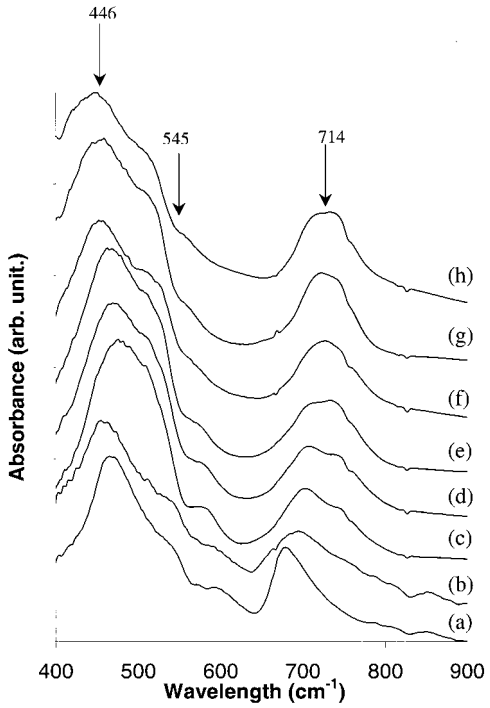

Figure 7. Evolution of the infrared spectra versus x in $Sr_{1-x}La_{1+x}Al_{1-x}Mg_xO_4$, $x = 0$ (a) to $x = 0.7$ (h).

Infrared Absorption. Figure 7 presents the infrared spectra of the samples for $x = 0$ (a) to $x = 0.7$ (h). Figure

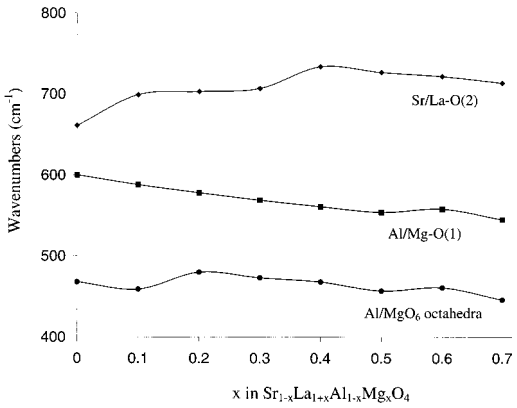

Figure 8. FTIR band frequencies plotted versus x in $Sr_{1-x}La_{1+x}Al_{1-x}Mg_xO_4$.

8 presents the plot of the evolution of the frequencies versus the substitutional ratio x. A wide band observed around 468 cm^{-1} in the spectrum of $x = 0$ is shifted around 446 cm^{-1} for $x = 0.7$. As observed by Byeon et al.,[35] this broad band can result from the random distribution of AlO_6 and MgO_6 octahedra in the perovskite layer. The shift of this band to low frequency is in agreement with the increase of the a parameter from 3.7564(1) Å for $x = 0$[28] to 3.84414(9) Å for $x = 0.7$.

Another band at 661 cm^{-1} for $x = 0$ shifts to 714 cm^{-1} for $x = 0.7$. This wide band corresponds to the stretching vibration of the Sr/La−O(2) bond along the c axis as confirmed by Singh et al.[36] and Ordier et al.[37] The assignment of the observed band at 600 cm^{-1} for $x = 0$ and at 545 cm^{-1} for $x = 0.7$ is not straightforward. The literature[36,37] proposes the Al/Mg−O(1) stretching mode.

Conclusion

The present studies show the refinement of the structure solid solution $Sr_{1-x}La_{1+x}Al_{1-x}Mg_xO_4$ in the $I4/mmm$ space group, which allows the estimation of the interatomic distances. These distances clearly traduce compression or dilation effects of the bond length in the lattice. These materials have been characterized by Raman and infrared spectroscopies. An assignment of the different bands is proposed on the basis of the results of the structural data and of the excitation wavelength. It is also observed that the number of bands in the Raman spectra is higher than predicted. An effect of local distortion of the octahedron Al/MgO_6 is suggested to explain this phenomenon. At last, the increase of the internal stresses against the substitutional ratio explain the decrease of structural stability of the solid solution, which follows the evolution of the t factor.

CM001209E

(35) Byeon, S.−H.; Demazeau, G.; Choy, J.−H. *Jpn. J. Appl. Phys.* **1995**, *34*, 6156.
(36) Singh, K. K.; Ganguly, P. *Spectrochim. Acta A* **1984**, *40*, 539.
(37) Ordier, P.; Leblanc, M.; Choisnet, J. *Mater. Res. Bull.* **1986**, *21*, 787.